

The sdB pulsating star V391 Peg and its putative giant planet revisited after 13 years of time-series photometric data ★ ★★

R. Silvotti¹, S. Schuh², S.-L. Kim³, R. Lutz⁴, M. Reed⁵, S. Benatti⁶, R. Janulis⁷,
L. Lanteri¹, R. Østensen⁵, T. R. Marsh⁸, V. S. Dhillon^{9,10}, M. Paparo¹¹, L. Molnar¹¹

¹ INAF-Osservatorio Astrofisico di Torino, strada dell'Osservatorio 20, 10025 Pino Torinese, Italy
e-mail: silvotti@oato.inaf.it

² Max Planck Institute for Solar System Research, Justus-von-Liebig-Weg 3, 37077 Göttingen, Germany

³ Korea Astronomy and Space Science Institute, Daejeon 34055, Korea

⁴ German Aerospace Center (DLR), Remote Sensing Technology Institute, Münchener Str. 20, 82234 Weßling, Germany

⁵ Department of Physics, Astronomy and Materials Science, Missouri State University, Springfield, MO 65897, USA

⁶ INAF-Osservatorio Astronomico di Padova, Vicolo dell'Osservatorio 5, 35122 Padova, Italy

⁷ Institute of Theoretical Physics and Astronomy, Vilnius University, Gostauto 12, Vilnius 01108, Lithuania

⁸ Department of Physics, University of Warwick, Coventry CV4 7AL, UK

⁹ Department of Physics and Astronomy, University of Sheffield, Sheffield S3 7RH, UK

¹⁰ Instituto de Astrofísica de Canarias, Via Lactea s/n, La Laguna, E-38205 Tenerife, Spain

¹¹ Konkoly Observatory of the Hungarian Academy of Sciences, Konkoly-Thege M. u 15-17, 1121, Budapest, Hungary

Received ... June 2017; accepted ...

ABSTRACT

V391 Peg (alias HS 2201+2610) is a subdwarf B (sdB) pulsating star that shows both p - and g -modes. By studying the arrival times of the p -mode maxima and minima through the O–C method, in a previous article the presence of a planet was inferred with an orbital period of 3.2 yr and a minimum mass of $3.2 M_{\text{Jup}}$. Here we present an updated O–C analysis using a larger data set of 1066 hours of photometric time series ($\sim 2.5\times$ larger in terms of the number of data points), which covers the period between 1999 and 2012 (compared with 1999–2006 of the previous analysis). Up to the end of 2008, the new O–C diagram of the main pulsation frequency (f_1) is compatible with (and improves) the previous two-component solution representing the long-term variation of the pulsation period (parabolic component) and the giant planet (sine wave component). Since 2009, the O–C trend of f_1 changes, and the time derivative of the pulsation period (\dot{p}) passes from positive to negative; the reason of this change of regime is not clear and could be related to nonlinear interactions between different pulsation modes. With the new data, the O–C diagram of the secondary pulsation frequency (f_2) continues to show two components (parabola and sine wave), like in the previous analysis. Various solutions are proposed to fit the O–C diagrams of f_1 and f_2 , but in all of them, the sinusoidal components of f_1 and f_2 differ or at least agree less well than before. The nice agreement found previously was a coincidence due to various small effects that are carefully analysed. Now, with a larger dataset, the presence of a planet is more uncertain and would require confirmation with an independent method. The new data allow us to improve the measurement of \dot{p} for f_1 and f_2 : using only the data up to the end of 2008, we obtain $\dot{p}_1 = (1.34 \pm 0.04) \times 10^{-12}$ and $\dot{p}_2 = (1.62 \pm 0.22) \times 10^{-12}$. The long-term variation of the two main pulsation periods (and the change of sign of \dot{p}_1) is visible also in direct measurements made over several years. The absence of peaks near f_1 in the Fourier transform and the secondary peak close to f_2 confirm a previous identification as $l=0$ and $l=1$, respectively, and suggest a stellar rotation period of about 40 days. The new data allow constraining the main g -mode pulsation periods of the star.

Key words. Stars: horizontal-branch – Stars: oscillations – Asteroseismology – Stars: individual: V391 Peg – Planets and satellites: detection – Planets and satellites: individual: V391 Peg b

1. Introduction

V391 Peg was the first case of a post-red giant branch star showing evidence of the presence of a planet (Silvotti et al. 2007 (hereafter SSSJ07), Silvotti 2008), indicating that giant planets may survive the first giant expansion of a star, provided that the orbital distance is large enough. For V391 Peg b, a minimum

* The complete set of data is available in electronic form at the CDS via anonymous ftp to cdsarc.u-strasbg.fr (130.79.128.5) or via <http://cdsweb.u-strasbg.fr/cgi-bin/qcat?J/A+A/>

** Based on observations obtained at the following observatories: WHT 4.2m, TNG 3.6m, Calar Alto 2.2m, NOT 2.5m, Loiano 1.5m, LOAO 1.0m, MDM 1.3m, Moletai 1.6m, MONET-North 1.2m, Piszkestető 1.0m, Mercator 1.2m, Wise 1.0m, Lulin 1.0m, Baker 0.6m.

mass of $3.2 M_{\text{Jup}}$ was found, with an orbital period of 3.2 yr, corresponding to an orbital distance of about 1.7 AU. The presence of the planet was inferred by measuring the arrival times of the maxima and minima of the stellar light, given that V391 Peg is a pulsating subdwarf B (sdB) star with at least four p -mode pulsation periods between 344 and 354 s (Silvotti et al. 2002, 2010), and a few longer-period g -modes (Lutz et al. 2009). A recent review on hot subdwarfs of spectral type O and B is given by Heber (2016).

V391 Peg b is not the first case in which the light travel-time delay is used to detect secondary low-mass bodies. In principle, the timing technique may be used on any star or stellar system that has a sufficiently stable clock, which may be given by the os-

cillations of the stellar flux in pulsating stars (like in this case), but also radio signals in pulsars or eclipse timing in eclipsing binaries. Radio timing was used to detect the first planetary system around the pulsar PSR 1257+12 (Wolszczan & Frail 1992). The extremely high precision of the radio pulse made it possible to detect PSR 1257+12 b, the Moon-mass innermost planet of the system (Konacki & Wolszczan 2003). Of the planets detected through eclipse timing, the most convincing case is given by two circumbinary planets orbiting the pre-cataclysmic binary NN Ser. Eight years after the discovery paper (Qian et al. 2009, see also Beuermann et al. 2010) and 26 years after the first data, their existence remains the best explanation for the observed eclipse time variations (Bours et al. 2016). Many other detached close binaries show eclipse time variations: for some of them, the presence of planets is excluded by dynamic stability computations and the periodic O–C trends may be caused by other reasons, such as Applegate-like mechanisms (Applegate 1992, Lanza 2006). However, for some others, the energy required to produce the quasi-periodic changes in the quadrupole moment of the secondary star referred to as the Applegate mechanism, is too high; and the presence of Jovian planets remains the most plausible explanation (Völschow et al. 2016).

The idea of using stellar pulsation to measure the reflex motion that is due to a companion is not new (e.g., Barnes & Moffett 1975). Recently, the high photometric accuracy achievable from space, in particular with the *Kepler* mission, has led to a renewed interest in this technique (Silvotti et al. 2011), and two systematic approaches based on frequency modulation (FM) and phase modulation (PM, equivalent to the O–C method) were proposed (Shibahashi & Kurtz 2012, Telting et al. 2012, Shibahashi et al. 2015; Murphy et al. 2014, 2016b).

However, to detect low-mass (substellar) companions, we need very stable pulsators. When we exclude all the solar-like oscillators, good candidates are the delta Scuti stars (Compton et al. 2016; see also recent discovery by Murphy et al. 2016a) and compact stars like white dwarfs or sdB stars. As for white dwarfs, many articles in the literature have addressed this issue (e.g., Kepler et al. 1991), but it has become increasingly evident that other effects are present that can mimic light travel time effects in the O–C diagrams of these stars (e.g., Dalessio et al. 2015). For sdB stars the situation looks more promising, perhaps because these stars have a fully radiative envelope, and there is at least one case in which the presence of a low-mass stellar companion detected from pulsation timing was confirmed by radial velocity measurements (Barlow et al. 2011b). Another recent case of a pulsation-timing detection of an F5V companion to an sdB pulsator is reported by Otani et al. (2017).

After the detection of V391 Peg b, some other planet or brown dwarf (BD) candidates orbiting sdB stars were proposed using different detection methods. From eclipse timing, about one-third of the known detached sdB/sdO+dM (dM=M-dwarf) post-common-envelope binaries (PCEB) are suspected to host planets/BDs: HW Vir (Beuermann et al. 2012 and references therein), HS 0705+6700 (alias V470 Cam, Qian et al. 2013 and references therein), HS 2231+2441 (Qian et al. 2010 and references therein; but see also Lohr et al. 2014), NSVS 14256825 (Almeida et al. 2013; Hinse et al. 2014 and references therein), NY Vir (Lee et al. 2014 and references therein), and 2M 1938+4603 (Baran et al. 2015). Interesting explorations on the origin of PCEB (and specifically sdB+MS/BD) circumbinary planets can be found in Zorotovic & Schreiber (2013), Schleicher & Dreizler (2014), Bear & Soker (2014), and Völschow et al. (2016). Very different planets or planetary remnants with terrestrial radii have been proposed from tiny reflec-

tion effects detected by the *Kepler* spacecraft in KIC 05807616 (Charpinet et al. 2011) and KIC 10001893 (Silvotti et al. 2014). However, none of these sdB planet/BD candidates has been confirmed with at least two independent detection methods. More robust detections of a few brown dwarfs (BDs) in eclipsing sdB binaries (also called HW Vir systems from the sdB+dM prototype) were obtained by combining stellar radial velocities (RVs) with photometric measurements: J08205+0008, J1622+4730 and V2008-1753 have companion masses of about 71, 67, and 69 M_{Jup} , respectively (Geier et al. 2011; Schaffenroth et al. 2014, 2015). At least two more sdB+BD eclipsing systems were recently found from the OGLE survey (Schaffenroth in preparation, private communication). Finally, two more BD candidates in sdB binaries were found by combining radial velocities (RVs) with photometric reflection effects: CPD-64°6481 and PHL 457, with minimum masses of 50 and 28 M_{Jup} , respectively (Schaffenroth et al. 2014b).

In this paper we reconsider the case of V391 Peg, for which we have collected six years of new photometric time-series data, increasing the number of data points by a factor of about 2.5. The main stellar parameters of V391 Peg are summarized in Table 1. We note that the JHK magnitudes are compatible with a single sdB star and do not indicate any near-IR excess.

In section 2 a short summary of the data acquisition and reduction is given, including the extraction of the pulsation frequencies. The analysis of the amplitude spectrum of the p -modes at different frequency resolutions is presented in section 3. Section 4 is dedicated to the O–C analysis of the two main p -modes. In section 5 we discuss the presence of the planet in the light of the new O–C results, including a perspective on future developments. In section 6 we present an analysis of the g -mode amplitude spectrum. Finally, a summary of our results is given in section 7.

Table 1. Stellar parameters.

U	13.35 ± 0.03^1
B	14.35 ± 0.02^1
V	14.57 ± 0.02^1
J (2MASS)	15.17 ± 0.05
H (2MASS)	15.16 ± 0.10
K (2MASS)	15.38 ± 0.20
T_{eff}	$29\,300 \pm 500 \text{ K}^2$
$\log g$	$5.4 \pm 0.1 \text{ (cgs)}^2$
$\log(\text{N}(\text{He})/\text{N}(\text{H}))$	-3.0 ± 0.3^2
M	$0.47^3 M_{\odot}$
$R=R(M, g)$	$0.23 R_{\odot}$
$L=L(T_{\text{eff}}, R)$	$34 L_{\odot}$
$M_V=M_V(L, BC)$	3.88^4
$d=d(V, M_V)$	$1\,400 \text{ pc}$

Notes: ¹ Our calibration at TNG.

² From Østensen et al. 2001.

³ SdB canonical mass (assumed), see e.g. Heber 2016.

⁴ Absolute V mag assuming a bolometric correction $BC=-2.95$.

2. Time-series photometric data: extraction of the pulsation frequencies

The new time-series photometric data were obtained using different telescopes and instruments (see Table 2) with at least one and often two or more comparison stars close to the target in order to remove spurious photometric modulations that are due to atmospheric transparency variations. The distribution of the data

Table 2. Time-series photometry.

Telescope/instrument	Observers	# runs	# hours
Previous data (1999–2006) ¹		168	421.3
Loiano 1.5m/BFOSC	RS	20	75.4
Piszkéstető 1.0m/CCD	MP/LM	14	67.5
Moletai 1.6m/CCD	RJ	26	79.4
Wise 1.0m/CCD	EL	6	35.7
Lulin 1.0m/CCD	WSH	7	24.2
MDM 1.3m/CCD	MR	7	33.4
LOAO 1.0m/CCD	SLK	47	134.1
Monet-N 1.2m/CCD	SS/RL	20	55.0
Baker 0.6m??/CCD	MR	4	11.5
Mercator 1.2m/CCD	RØ+students	24	69.8
WHT 4.2m/ULTRACAM	TRM/VSD	7	36.7
NOT 2.6m/ALFOSC	RØ	3	11.2
TNG 3.6m/DOLORES	RS	8	18.7
Calar Alto 2.2m/CAFOS	SS/RL	10	25.9
Tot new data (2007–2012)		203	644.9 ²
All data (1999–2012)		371	1066.2

Notes: ¹ See SJJ07 Supplementary Information for more details (a Monet-N run of Nov 2006 was added to that list).

² This number is smaller than the sum of col. 4 given that sometimes overlapping data from different telescopes were averaged using a weighted mean.

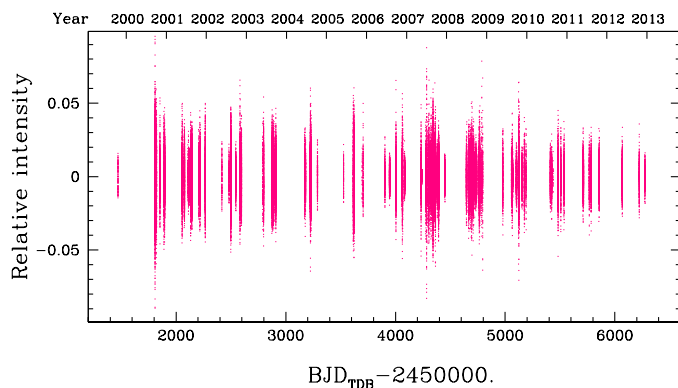


Fig. 1. Distribution of the 217,232 data points over 13 years. The overall duty cycle is 0.92%, and the best coverage is obtained in 2007 with a duty cycle of 5.55%. The varying relative intensity is caused by the beating between the main frequencies and also depends on the varying quality of the data.

during the 13 years of observation is shown in Fig. 1. Most of the data were taken using a standard Johnson B filter. Only at NOT and MERCATOR did we use a Bessell B and a Geneva B filter, respectively. Moreover, a SLOAN g filter was used in the WHT-MDM run of October 2007¹. The data obtained in October 2007 at the Piszkéstető, Loiano, and Lulin Observatories were collected without any filter in order to maximize the signal-to-noise ratio (S/N) of that run. The differences introduced by the different filters in terms of amplitudes or phases of the pulsation modes were considered and found to be negligible because of the much larger volume of standard B measurements. From nonadiabatic models, these differences (in particular the phase differences) are expected to be very small for $l=0$ and $l=1$ modes (Randall et al. 2005; see in particular their Figs. 13 and 14). The

¹ The WHT data were simultaneously obtained with ULTRACAM in three photometric bands (u, g, and r) but only the g-band data are used in this article, while multi-band data were previously used to identify the main pulsation modes of V391 Peg (Silvotti et al. 2010).

data were reduced mainly by the observers using standard procedures for aperture differential photometry. The times of all the data (new and old) were converted into Barycentric Dynamical Times (BJD_{TDB}) following Eastman et al. (2010)).

From the reduced data we extracted accurate pulsation frequencies using a classical prewhitening technique: an iterative Fourier transform (FT) process was applied subtracting the main frequency from the data residuals at each iteration, until no frequencies with amplitudes larger than four times the FT mean noise level were present. At the end of this iterative process, the pulsation frequencies, amplitudes, and phases were optimized through a multi-sinusoidal fit, whose results are given in Table 3. Appropriate statistical weights were set and considered in the sinusoidal fits of the p -modes (Silvotti et al. 2006) in order to take the varying quality of the data into account that is due to different telescope apertures, instrument efficiencies, and weather conditions.

3. P-modes

The first problem in analyzing a data set of several years is that the pulsation frequencies are no longer constant. This was already known for V391 Peg, and a quantitative measurement of \dot{p} had been obtained from previous data giving $\dot{p}=1.46\pm 0.07\times 10^{-12}$ and $2.05\pm 0.26\times 10^{-12}$ for f_1 and f_2 , respectively (SJJ07). In general, the time variation of a pulsation frequency gradually broadens the width of the peak in the Fourier transform and may split it into different close peaks if the data set is long enough. For a linear frequency variation, the time needed to split a pulsation frequency into different close peaks is given by

$$T \approx P \left(\frac{1.5}{\dot{p}} \right)^{1/2}, \quad (1)$$

where P is the pulsation period, and the value 1.5 comes from the actual frequency resolution, given by $\sim 1.5/T$ (Loumos & Deeming 1977). For V391 Peg we obtain $T \approx 10$ years. However, after a few years, this effect already becomes important and makes the standard prewhitening technique (which assumes fixed frequencies and amplitudes) less efficient in returning precise frequencies. For this reason, after several tests we decided to split our analysis of the amplitude spectrum into three steps with data sets of different length and different frequency resolution.

It is useful to recall here that the two main pulsation modes of V391 Peg were identified as $l=0$ and $l=1$ from high-precision multi-color photometry obtained with ULTRACAM at the WHT (Silvotti et al. 2010). We show below that this identification is well supported by the current analysis.

3.1. Low-frequency resolution: main pulsation frequencies

As a first step, we consider our best-quality run of October 2007, with a length of 7.9 days and a duty cycle of 35%. At this level of frequency resolution, $\delta f \approx 2.2 \mu\text{Hz}$, the amplitude spectrum is very clean and shows only four pulsation modes without any trace of multiplets of close frequencies (Fig. 2).

3.2. Medium-frequency resolution: rotational splitting of f_2 ?

As a second step, we consider a larger data set of about 220 days, collected in 2007. This data set is a compromise between best duty cycle, best data quality, and relatively long duration in order to detect possible rotational splitting of the pulsation modes

Table 3. Pulsation frequencies.

		\bar{F} [μHz]	\bar{P} [s]	\bar{A} [ppt] ¹	Phase ²
<i>p</i>-modes³	f_1	2860.938272(06)	349.5356784(07)	7.56	0.7327(06)
	f_2	2824.096225(10)	354.0955832(13)	4.06	0.7492(11)
	f_3	2881.123233(62)	347.0868544(74)	0.77	0.3285(58)
	f_4	2909.995332(63)	343.6431630(75)	0.65	0.2560(58)
	f_2^-	2823.932963(57)	354.1160549(72)	0.93	0.1015(54)
<i>g</i>-modes⁴	F_1	201.96312(16)	4951.3991(40)	1.01	0.116(09)
	F_2	295.11065(23)	3388.5596(26)	0.78	0.475(12)
	F_3	320.19726(23)	3123.0748(22)	0.71	0.918(13)

Notes: ¹ ppt = parts per thousand = 0.1%.

² Normalized phases corresponding to $\text{BJD}_{\text{TDB}} 2451470.476568$ (1st datum).

³ For the *p*-modes, frequencies and periods are the mean values in the period 1999–2012, corresponding to $\text{BJD}_{\text{TDB}} \sim 2454090$ (or year ≈ 2007.0), which is the weighted mean time. We note that in 10 years of observation, the secular variations of the pulsation frequencies and periods are larger than the 1σ errors reported here, obtained from a Monte Carlo simulation assuming constant frequencies.

⁴ Because of the noise in the Fourier transform at low frequencies (Fig. 11), the multi-sinusoidal fits for the *g*-modes are less stable than those for the *p*-modes, and therefore the 1σ frequency/period errors for the *g*-modes reported here are underestimated.

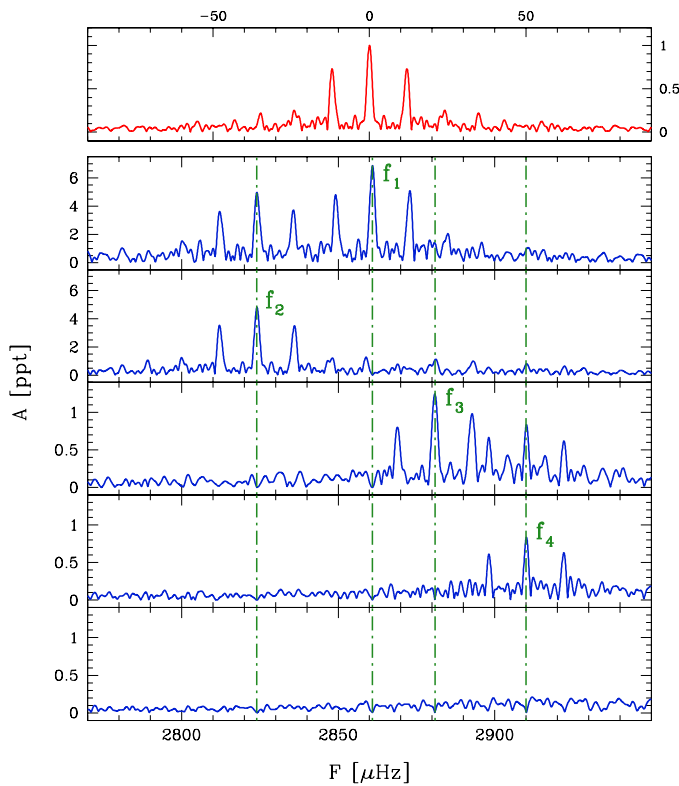


Fig. 2. *P*-mode amplitude spectrum of our best-quality run of 7.9 days, with a duty cycle of 35%, obtained in October 2007 with a SLOAN g filter using two telescopes at different longitudes: the WHT 4.2m in La Palma, equipped with ULTRACAM, and the MDM 1.3m at Kitt Peak. The upper panel shows the spectral window (red), while the other panels from top to bottom show the amplitude spectra of the data and of the residuals after one, two, three, and four prewhitening steps. A plot showing the high quality of the ULTRACAM data is presented in Silvotti et al. (2010).

with $l > 0$. At the same time, with 220 days, the effects of the long-term variations of the pulsation frequencies are still small, which keeps the amplitude spectrum relatively clean (Fig. 3). When we removed the four main pulsation frequencies through prewhitening, two low-amplitude peaks emerged from the noise, close to f_2 and f_3 , while nothing appeared close to f_1 , which confirms that this must be an $l=0$ mode. The peak close to f_3 (f_3^+) is only

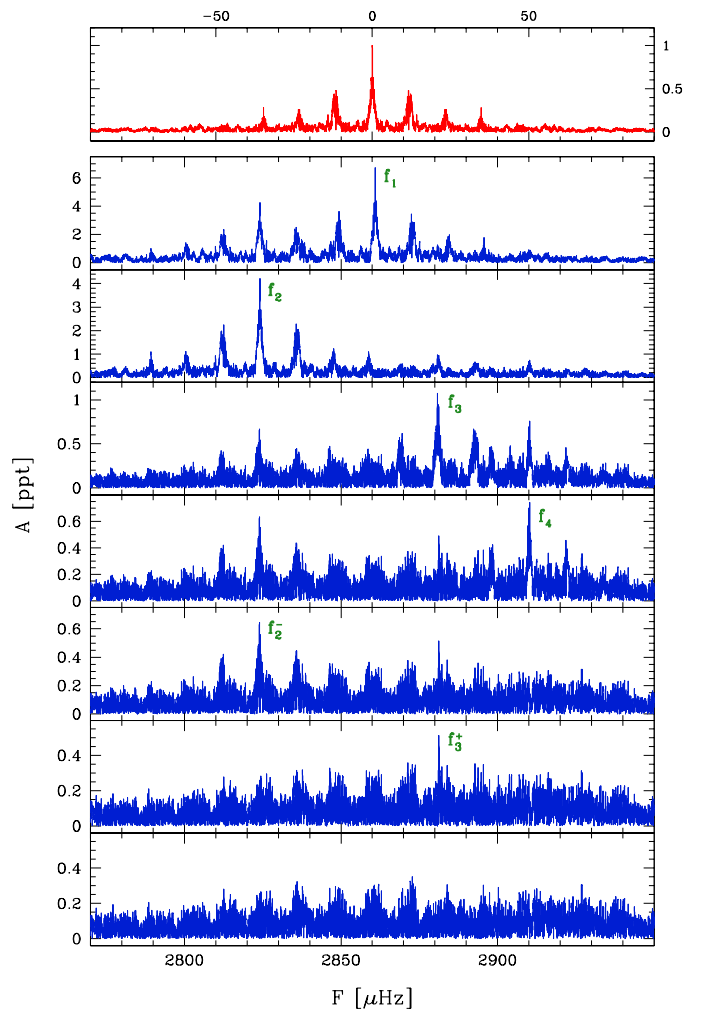


Fig. 3. Same as Fig. 2, but using all the data of 2007, the year with the best coverage. Thanks to the increased frequency resolution, we see that after four prewhitening steps, there is still significant power, with secondary peaks near f_2 and f_3 that may be due to the rotational splitting of these modes.

$\sim 3.4\sigma$ above the noise, which is below our detection threshold of 4σ . Secondary peaks close to f_3 are also visible when we use the whole data set (1999–2012), but with a very low S/N. The

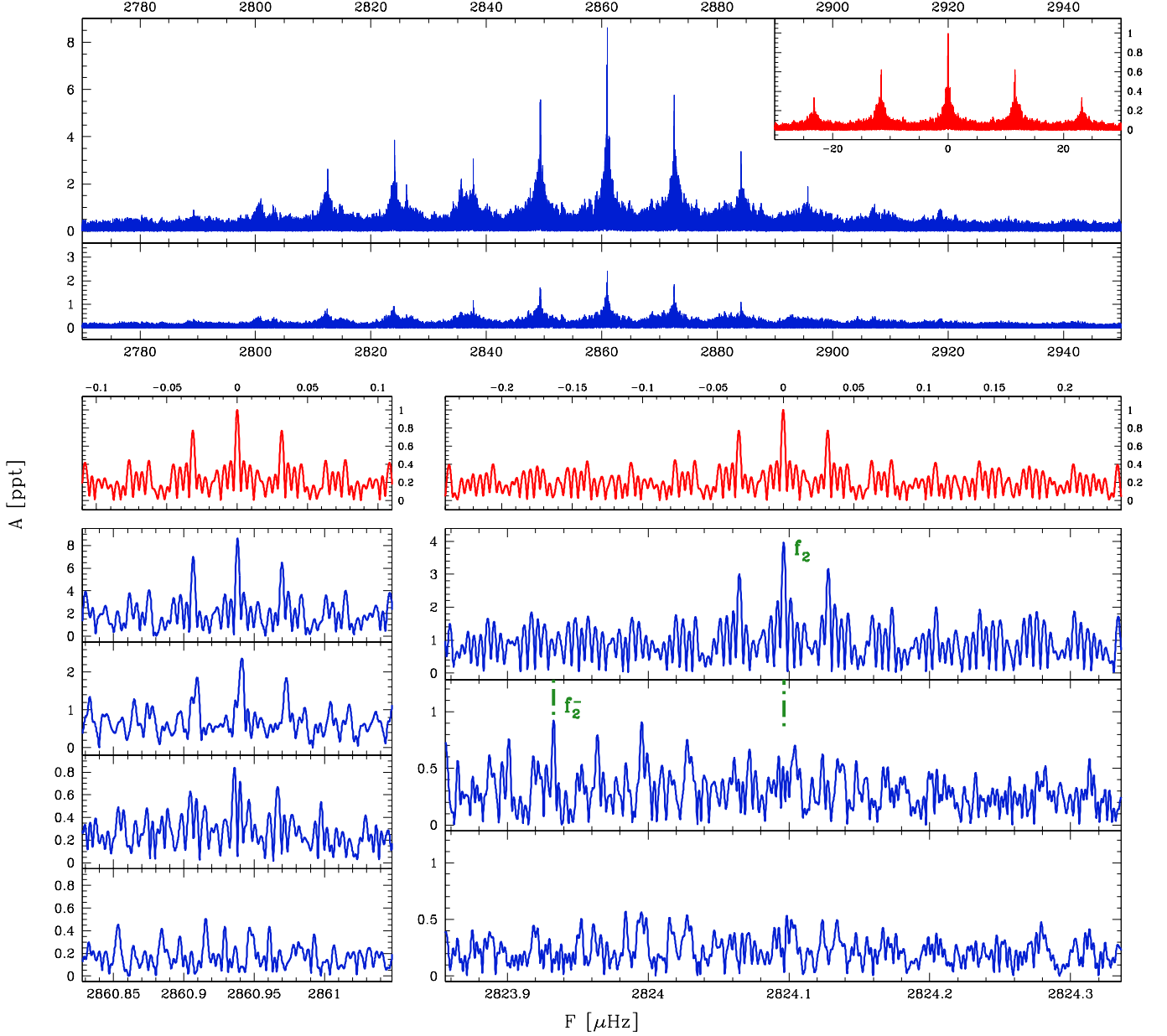


Fig. 4. Same as Figs. 2 and 3, but using the whole data set (1999–2012). Upper panels: amplitude spectrum of the data and of the residuals (on the same vertical scale) after subtracting the four main pulsation frequencies (f_1 to f_4). We note that the residual power is significantly higher than in Fig. 3. The small box shows the normalized spectral window (red) with the one-day aliases at $\pm 11.57 \mu\text{Hz}$. Lower panels (from top to bottom): normalized spectral window (red) with the one-year aliases at $\pm 31.7 \text{ nHz}$, and details of the amplitude spectrum of data and residuals near f_1 (left) and f_2 (right). The horizontal scale in the left and right panels is the same. Two vertical dashed lines (green) highlight two components of a possible rotational splitting. See text for more details.

peak close to f_2 (f_2^-), at about 4.3σ above the noise, differs by $-0.181 \mu\text{Hz}$ from f_2 and is also detected in the whole data set, but at a lower S/N and smaller separation of $-0.163 \mu\text{Hz}$ (Fig. 4 lower right panel). Using the latter separation, which is more precise, and assuming that f_2^- is part of an $l=1$ triplet split by stellar rotation in which f_2 is the central component, we obtain a stellar rotation period of about 40 days. This value is obtained in the slow rotation approximation ($\Omega_{\text{ROT}} \ll f$, see Ledoux 1951),

$$f_{k,l,m} = f_{k,l,0} + m \Omega_{\text{ROT}} (1 - C_{k,l}), \quad (2)$$

in which we have used a value of 0.43 for the Coriolis term $C_{k,l}$ according to the adiabatic evolutionary models by Charpinet et al. 2002 (the model that fits best T_{eff} , $\log g$ and P of V391 Peg

is model 19 of sequence 4). The low amplitude of the secondary peak suggests a low inclination. This interpretation is consistent with the previous identification of f_2 as an $l=1$ mode by Silvotti et al. (2010). A rotation period of ~ 40 days would be compatible with the distribution of rotation periods as recently measured by the *Kepler* spacecraft in a sample of 18 sdB g -mode pulsators (see Zong 2017 and references therein). Thirteen of them show periods between 6 and 88 days, with a mean value of about 33 days. The other five do not show any rotational splitting of the frequencies, indicating that they may have very low inclinations and/or extremely long rotation periods.

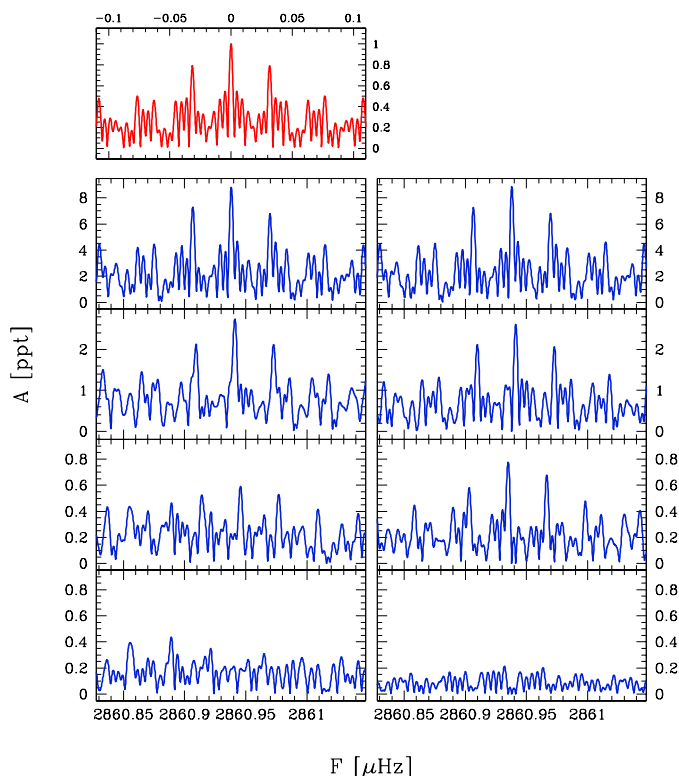


Fig. 5. Comparison between the amplitude spectrum near f_1 of the data (left) and the amplitude spectrum near f_1 of a simulated data set (right) with the same time distribution. In this test we used only the data up to 2009.0 because in this period it is easier to simulate the behavior of f_1 . For the simulated data we used a single pure sine wave (no noise) with the same frequency and amplitude of f_1 and also with similar long-term frequency and amplitude variations (linear variation of the period with $\dot{p}=1.34\times 10^{-12}$, as derived by the O–C analysis, and sinusoidal variation of the amplitude like in Fig. 7 upper right panel, green section). Like in the previous figures, the upper left panel is the normalized spectral window (red), while the other panels are the amplitude spectra of data and residuals after one, two, and three prewhitening steps. This simple test shows that up to the secondary peak on the right side of f_1 , the data are well reproduced by the simulation, both in terms of frequency and amplitude. See text for more details.

3.3. High-frequency resolution: frequency and amplitude variations

When we further increase the length of the data set and consider the whole light curve in the period 1999–2012, the amplitude spectrum is much more complex because of the effects of the frequency variations, which become important (Fig. 4). When we subtract the main pulsation frequencies from the light curve through prewhitening, secondary peaks emerge very close to the main pulsation frequencies. The reason is that prewhitening subtracts from the data at each step a sine wave with constant frequency and amplitude, while on timescales of many years, pulsation frequencies and amplitudes are no longer constant. This effect, which is well visible for f_1 (Fig. 4 lower left panels), adds noise to the amplitude spectrum of the residuals and may lead to incorrect determinations of the low-amplitude frequencies. In this respect, the average values of f_3 and f_4 might be slightly different from those reported in Table 3, with differences even larger than the errors reported there.

In order to decipher the information contained in the peaks close to f_1 , we conducted a small experiment with a synthetic

light curve. Since the behavior of f_1 is fairly regular and relatively easy to model in the period up to 2009.0, while it becomes more irregular later on (see Figs. 7, 8, and 9), we considered only the period up to 2009.0. The synthetic light curve contains a single sine wave without noise with the same time distribution as the data, a frequency and amplitude equal to f_1 , and similar frequency and amplitude variations. In practice, we imposed a linear variation of the period with $\dot{p}=1.34\times 10^{-12}$ (the value found from the O–C analysis described in section 4) and a sinusoidal variation of the amplitude corresponding to the sinusoidal fit shown in Fig. 7 (top right panel). The amplitude spectrum of this synthetic light curve near f_1 is shown in Fig. 5 (right panels) and can be compared with the real data in the left panels. Up to the secondary peak on the right side of f_1 , the agreement between real and synthetic data is very good both in terms of frequency and amplitude: we obtain $2860.9418\ \mu\text{Hz}$ and $2.74\ \text{ppt}$ vs $2860.9414\ \mu\text{Hz}$ and $2.61\ \text{ppt}$, respectively (the main peak being at $2860.9382\ \mu\text{Hz}$ with an amplitude of $8.84\ \text{ppt}$). Thus we verified that a linear time variation of a pulsation period splits the frequency into three close peaks almost equally spaced in frequency. If the amplitude is constant, the two secondary peaks have the same amplitude. If the amplitude is variable as in this case, the two secondary peaks have different amplitudes.

Before proceeding with our analysis on frequency and amplitude variations, it is important to verify that the uncertainties associated with frequencies and amplitudes such as those reported in Table 3 are correctly estimated. These uncertainties are the 1σ errors obtained from a Monte Carlo (MC) simulation on 1000 synthetic light curves in which random Gaussian noise (at the same level as the data) was added to the five p -modes listed in Table 3. In Fig. 6 the distribution of frequencies and amplitudes obtained from the MC simulations is shown for the two main pulsation modes of V391 Peg (f_1 and f_2).

After we verified that the error bars of our measurements were reliable, we measured the pulsation periods and amplitudes for f_1 and f_2 in each observing season (Fig. 7), where observing season means the period from May to December of the same year in which V391 Peg is observable. The frequencies and amplitudes shown in Fig. 7 were obtained from multi-sinusoidal fits considering only four frequencies (f_1 to f_4), while f_2^- was excluded because it is not detected in most of these one-season runs. The same exercise was repeated using all five frequencies, but the results were less reliable.

When we consider only the data up to 2009.0, corresponding to the green part of Fig. 7, the variation of p_1 can be fit with a straight line whose slope corresponds to $\dot{p}_1=(1.60\pm 0.20)\times 10^{-12}$. In the same period, the amplitude a_1 shows a fairly regular sinusoidal pattern with a period of about 3400 days (9.3 yr) and an amplitude of 29%. After 2009.0, the trend of the period and amplitude variations of p_1 changes and p_1 starts to decrease. The reason for this behavior, which is also confirmed by the O–C analysis in Figs. 8 and 9, is not known. Although we normally attribute period and amplitude variations to nonlinear interactions between different pulsation modes, in this case, with an $l=0$ mode, we cannot invoke the resonant mode coupling between the components of a multiplet of modes split by the stellar rotation, nor even the three-mode resonance, which would require that f_1 corresponds to a linear combination of the other two pulsation modes that we do not see. These two mechanisms were recently invoked as a possible explanation for the frequency and amplitude variations observed in the sdB g - and p -mode pulsator KIC 10139564 (Zong et al. 2016). The lower left panel of Fig. 7 shows that when we use all the available data, the variation in p_2 can be fit with a straight line whose slope corresponds

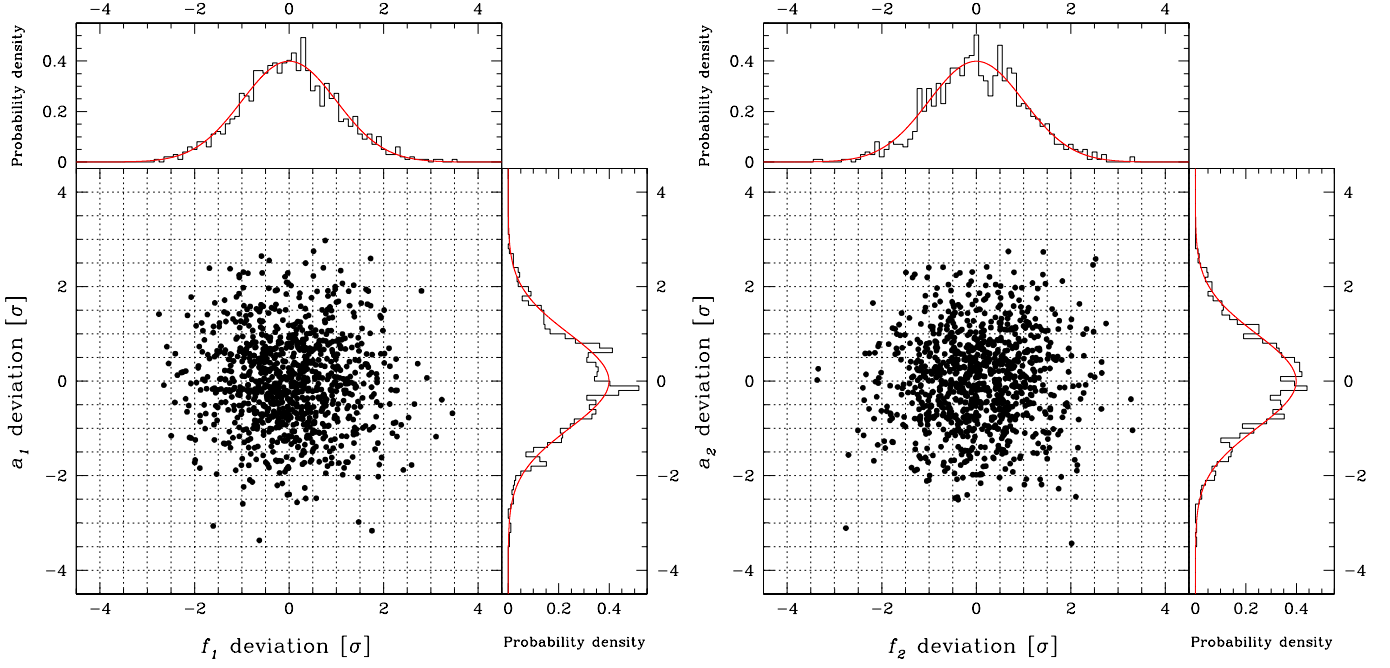


Fig. 6. Distribution of the frequency and amplitude deviations for the two main pulsation modes of V391 Peg. The deviations, in units of 1σ errors, are the differences between the values obtained from the original light curve and those obtained from 1000 artificial light curves created by the MC simulator of Period04 (Lenz & Breger 2005). The synthetic light curves are built using the five p -modes of Table 3 and adding Gaussian noise at the same level as the original data. The 2D distributions are also projected into 1D histograms and compared with a normal distribution (red).

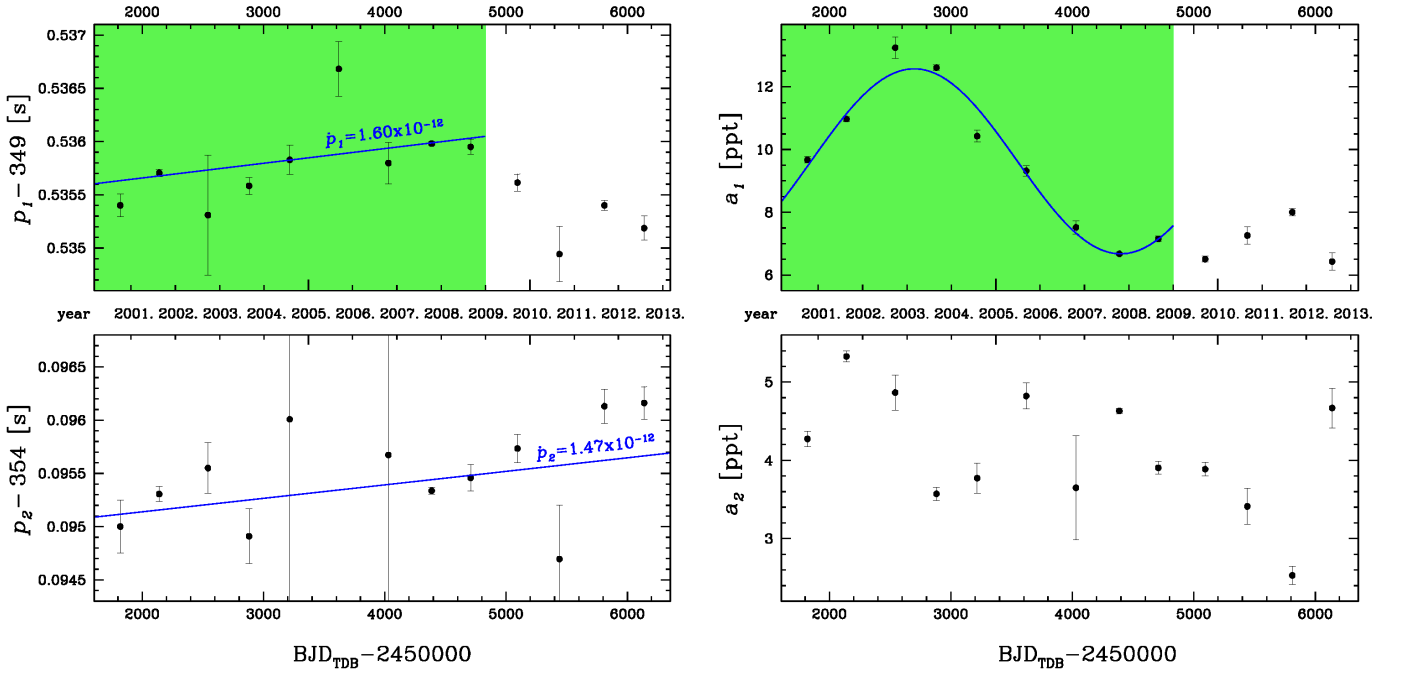


Fig. 7. Period and amplitude variations of the two main pulsation modes of V391 Peg. The variation of p_1 is compatible with a linear increase up to 2009.0, when a change of regime appears. The same change is also visible for the amplitude: up to 2009.0, a_1 shows a fairly regular sinusoidal shape with a period of about 3400 days or 9.3 years. A linear increase of the pulsation period is visible also for p_2 when considering the whole data set, while the irregular variations of a_2 can be at least partially attributed to the beating between f_2 and f_2^- . More details are given in the text.

to $\dot{p}_2 = (1.47 \pm 0.41) \times 10^{-12}$. In the lower right panel we see quite irregular variations of a_2 , but these apparent variations can be at least partially attributed to the interaction (beating) between f_2 and f_2^- . When we also consider f_2^- in the fit, the individual measurements of a_2 may vary by several tenths of ppt, indicating that the 1σ error bars of a_2 are underestimated. At shorter timescales,

we did not find any periodicity in the amplitude variations of a_2 that could confirm the beating effect and thus the rotation period of the star around 40 days. The mean quality of the data is not sufficient for detecting this effect. Based on our best-quality run of October 2007 at the WHT-MDM, we can only exclude short timescale variations (from night to night) for both a_1 and a_2 .

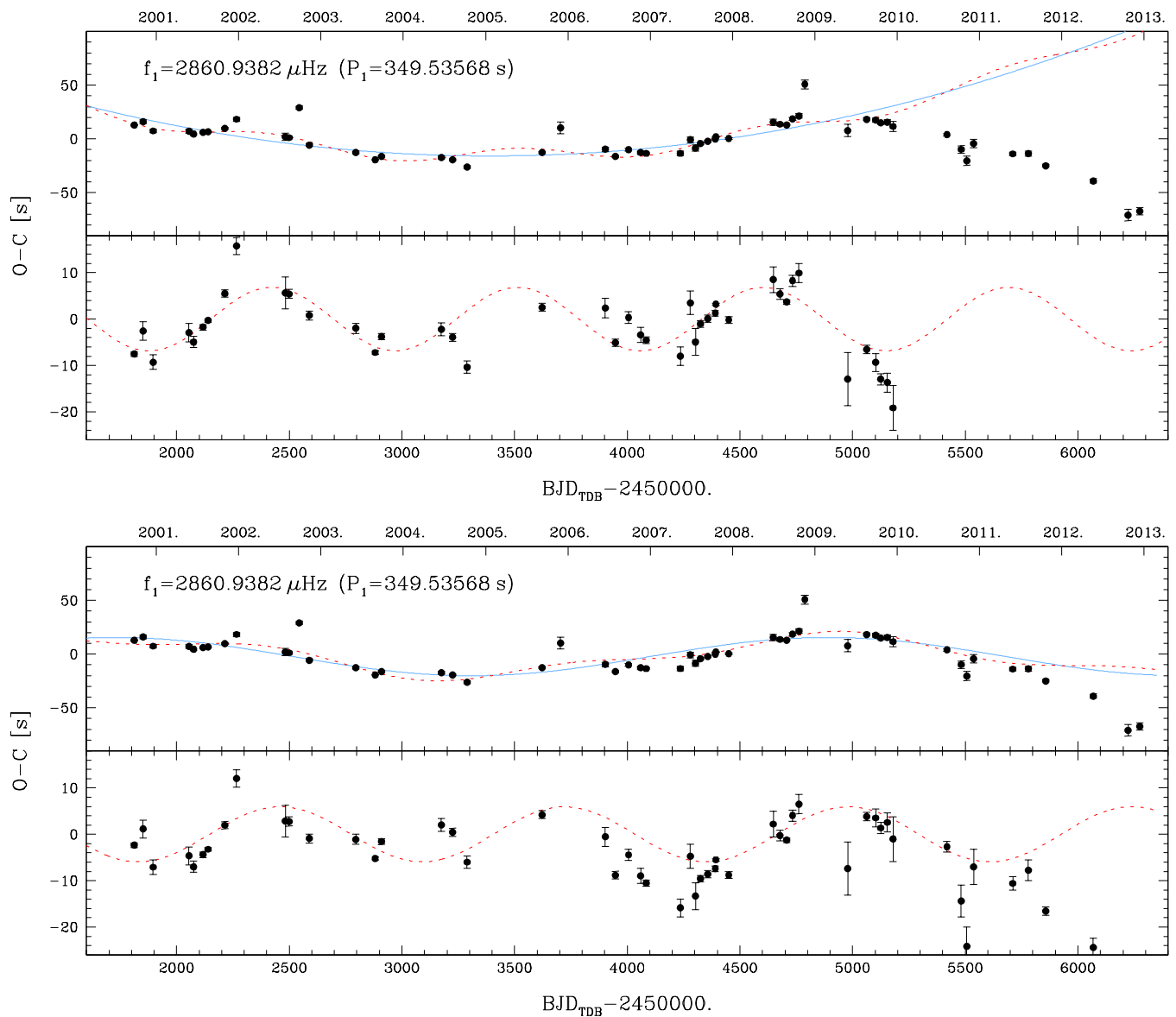


Fig. 8. O–C diagram of the main pulsation mode of V391 Peg when using monthly runs (each point represents the data collected within one month). Upper panels: fit of the O–C data with a parabola (long-term variation, blue continuous line) plus a sine wave (“planetary component”, red dashed line) and planetary component alone after subtracting the long-term component. This solution gives satisfactory results only up to the end of 2008, and the fit was made considering only the data up to 2009.0. Lower panels: same as upper panels, but using two sinusoids. In this case, the fit was made using all the data, but a reasonable fit is obtained only up to ~ 2010 , indicating that two components are simply not enough to obtain a reasonable fit of all the data. When we compare the planetary component alone in the period 2000–2009.0, the fit is better when we use parabola + sine wave ($\chi^2=762$) with respect to the double sine wave ($\chi^2=1267$); for comparison, a straight line would give $\chi^2=1376$.

We also attempted to fit the data from 1999 to the end of 2008 with two sine waves corresponding to f_1 and f_2 , leaving as free parameters not only the frequencies, amplitudes, and phases, but also \dot{p}_1 and \dot{p}_2 . The fit converged only when we fixed \dot{p}_2 , but the value that we obtained for \dot{p}_1 is about ten times higher than the value obtained from the direct measurements. This method is less reliable than the direct method or the O–C method described in the next section because it makes use of constant amplitudes, but we know that the amplitudes are not constant, and in particular, a_1 varies significantly (Fig. 7).

While amplitude variations in sdB p -mode pulsators have been known for a long time, with time scales ranging from days to years, the results reported in this section show that even the frequencies are less stable than previously believed and may suf-

fer significant variations that are not simply due to the long-term modifications of the stellar structure. Amplitude and frequency variations have recently been detected in most of the sdB pulsators observed by the *Kepler* spacecraft, with complex patterns that sometimes are stochastic (Østensen et al. 2014) and sometimes more regular and periodic (e.g., Zong et al. 2016).

4. O–C analysis

The O–C analysis (Sterken 2005; and subsequent articles in the same volume) is a powerful method for detecting tiny variations of the pulsation periods on long timescales that cannot be seen or clearly seen from direct independent measurements (like in Fig. 7). The O–C method is more sensitive than the direct method

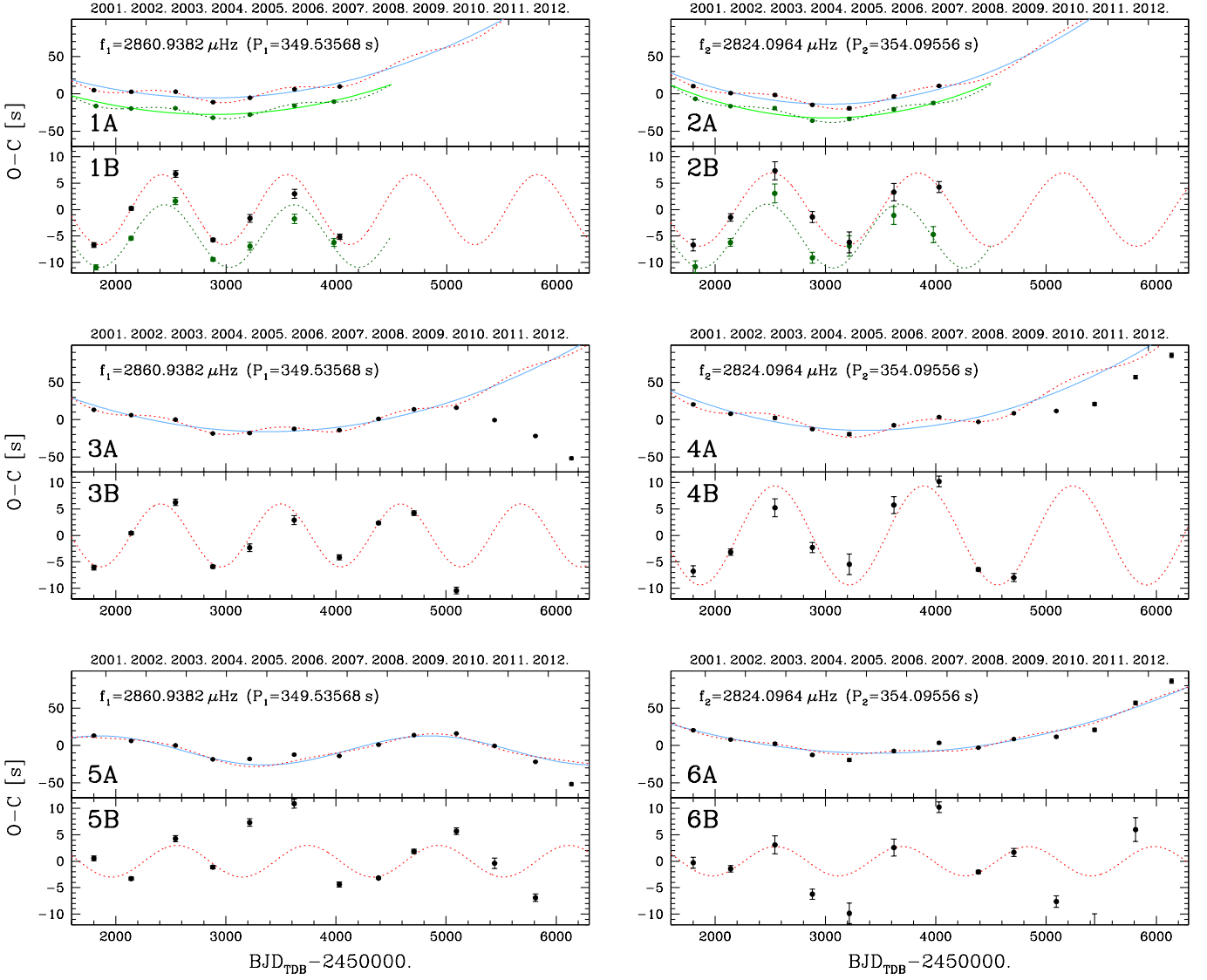


Fig. 9. Same as Fig. 8 for f_1 (left) and f_2 (right) for one-season runs. Panels 1A, 1B, 2A, and 2B are obtained using only the data up to 2007.0, so that we can directly compare the current results (blue and red lines) with those obtained by SSJ07 (green lines shifted by -20 s and -5 s in panels 1A and 2A and 1B and 2B, respectively). The small horizontal shifts of the first and last points are due to the addition of three observing runs that were not present in SSJ07. Panels 1B and 2B show that in the current results, the period of the sinusoid is slightly shorter for f_1 but longer for f_2 , so that at the end the agreement between f_1 and f_2 is worse with respect to SSJ07. The reasons of these differences are discussed in the text. When we add the new data, the longer period of the sinusoidal component of f_2 with respect to f_1 is confirmed (panels 3B and 4B), and moreover, we note a further difference in amplitude. Panel 3A confirms the change of regime of f_1 near 2009 that was already visible in Figs. 7 and 8. This change also tends to worsen the fit of f_2 (4A), and for this reason, the fits shown in panels 3A to 4B are obtained considering only the data up to 2009.0. Panels 5A and 5B show an alternative solution obtained using a low-frequency sine wave for the long-term component of f_1 , as in the lower panels of Fig. 8. The fits shown in panels 5A to 6B were obtained using all the available data. More comments are given in the text.

because instead of directly measuring the period change, it measures the phase variations induced by the period change. When we consider a period that changes linearly in time (a good approximation on timescales of a few years, extremely short with respect to the evolutionary timescales), the phase variations have the great advantage of being proportional to T^2 , where T is the duration of the observation.

In order to reduce the phase errors, the data for the O-C analysis were considered in monthly subsets. A four-sinusoid fit was applied to each subset using the best (fixed) frequencies from Table 3 (f_1 to f_4) and leaving amplitudes and phases as free parameters. f_2^- was not used because it is not detected in the monthly subsets.

The difference between these monthly phases and those obtained from the whole data set are the O-C differences shown in Fig. 8, in which the phase differences have been converted into time differences. In Fig. 8 we see the same effect as was already seen in Fig. 7: since 2009, the curvature in the O-C diagram of f_1 changes. We do not know the reasons for this change, it might be related to nonlinear interactions between different pulsation modes. In any case, it is clear from Fig. 8 (upper panels) that a two-component fit with a parabola plus a sinusoid (like in SSJ07) can give satisfactory results only up to ~ 2009 . When considering only the data up to 2009.0, the long-term parabolic variation of the main pulsation period corresponds to $\dot{P}_1 = (1.36 \pm 0.06) \times 10^{-12}$. In order to also fit the more recent data,

we tried a different approach using two sinusoids (lower panels of Fig. 8). Even in this way, we did not obtain a reasonable fit of the whole data set, and moreover, the quality of the fit up to 2009 is lower, indicating that a sinusoidal \dot{p} is not the solution.

As a second step, the O-C analysis was repeated using larger data subsets covering a whole observing season (that is, from May to December for V391 Peg) and using the same pulsation frequencies as before. Again, f_2^- was not used because it is not detected in almost all runs. These larger subsets are particularly useful for f_2 (the secondary pulsation frequency), in order to reduce the phase errors that are very large when we use the monthly subsets. The results are shown in Fig. 9. In the upper panels (from 1A to 2B), we see the O-C diagram of f_1 and f_2 when using only the data from 1999 to 2007.0, basically the same data as in SSJ07 (only three short runs were added), but with the new updated frequencies. These plots show that when we use better values for f_3 and f_4 , the sinusoidal components of f_1 and f_2 (panels 1B and 2B) differ: even if the amplitudes and the initial phases are still in agreement (like in SSJ07), the periods are now different. In the central panels (from 3A to 4B), we see the new fits when we use the data from 1999 to 2009.0, before the change of sign of \dot{p}_1 : the sinusoidal components of f_1 and f_2 (panels 3B and 4B) are similar to the previous ones (panels 1B and 2B), except for a larger amplitude for f_2 , which increases the differences between f_1 and f_2 . The parabolic components (panels 3A and 4A) correspond to $\dot{p}_1 = (1.34 \pm 0.04) \times 10^{-12}$ and $\dot{p}_2 = (1.62 \pm 0.22) \times 10^{-12}$, in good agreement with the previous measurements of SSJ07. These numbers also agree with adiabatic theoretical expectations for the secular variation of the pulsation periods (Charpinet et al. 2002). However, the fact that \dot{p}_1 changed sign near 2009 indicates that in real stars, these processes may be more complicated. Finally, in the lower panels of Fig. 9 (from 5A to 6B), we show the best two-component fits of the whole data set using two sinusoids with different periods for f_1 , and a parabola plus a sinusoid for f_2 . Except for the last points, these fits can reproduce the general trend of the O-C data (panels 5A and 6A), but show a large dispersion, particularly for f_1 : the sinusoidal fits in panels 5B and 6B (chi-squared equal to 894 and 276, respectively) are only slightly better than a simple straight line ($\chi^2 = 1075$ and 322). At the same time, the two sinusoidal components have similar periods, amplitudes, and phases within 4%, 8%, and 7% respectively.

In order to explore this in more detail, we made a weighted average of the O-C data in panels 5B and 6B (which means a weighted average of the O-C data of f_1 and f_2 after subtracting their long-term component). The result is illustrated in Fig. 10 and shows that when we sum the information from f_1 and f_2 , the fit of the sinusoidal component improves, and at the end, we have 9 points out of 13 that are consistent with a sine wave with a period of 1127 ± 45 days (or 3.09 ± 0.12 years) and an amplitude of 3.02 ± 0.85 light seconds. Assuming that the sine wave is caused by the planet and that the mass of the sdB star is $0.47 M_\odot$, these numbers correspond to an orbital distance of 1.6 AU and a minimum mass of $1.8 M_{\text{Jup}}$.

Although not shown in Fig. 9, we also tried to fit the O-C plots of f_1 and f_2 with a parabola plus two sinusoids (corresponding to two potential planets), but we were unable to find any solution for which the six parameters of the two sinusoids were in reasonable agreement between f_1 and f_2 .

Several checks were made in order to ensure that the new O-C results reported in this section are correct and robust and to understand why in SSJ07 periods, amplitudes, and phases of the sinusoidal components of the O-C diagrams of f_1 and f_2 agreed so well. As stated previously, the current O-C results

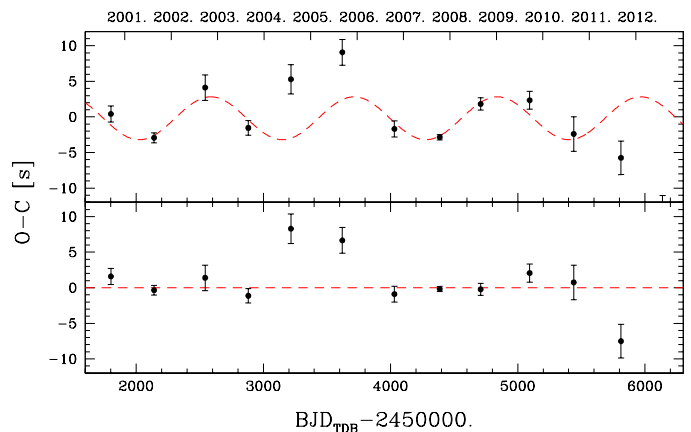


Fig. 10. O-C diagram obtained by combining the information from f_1 and f_2 . In practice, we have computed the weighted average of the points in panels 5B and 6B of Fig. 9 and recomputed the best fit with a sine wave. Compared with these panels, the fit is significantly improved and the residuals of 9 points out of 13 (including all those with smaller error bars) are close to zero.

were obtained using four frequencies (f_1 to f_4), also including the data taken with filters different from Johnson B, and making use of statistical weights. However, we also tested different combinations without statistical weights, excluding all the data taken in filters different from Johnson B (see section 2), and considering only the two main frequencies f_1 and f_2 . In all these tests, the results varied little². Thus it is not easy to understand the differences between our current results and those obtained in SSJ07 (even in that analysis, similar tests with different combinations were made). We conclude that the good agreement found in SSJ07 was a coincidence due to a few small differences between the two analyses: slightly different pulsation frequencies, two NOT observing runs that were excluded in SSJ07 because they were taken with a Bessell B filter and that are now included (after careful tests of the effects on phase and amplitude), and one new standard-B-filter Monet-N observing run that was not yet available in SSJ07. Of these factors, the greatest is probably given by the different frequencies that were used. In SSJ07 we used $f_1 = 2860.9387$, $f_2 = 2824.0965$, $f_3 = 2880.6842$, $f_4 = 2921.8463$, and $f_5 = 2882.0039 \mu\text{Hz}$. Comparing these values with those in Table 3, we see very small differences for f_1 and f_2 , compatible with real period variations; the new value of f_3 is higher by $0.4390 \mu\text{Hz}$; f_5 is not confirmed and used not at all in the new analysis, but its influence must be small because of the very low amplitude. Finally and mostly important, the updated value of f_4 is lower by $11.8510 \mu\text{Hz}$ with respect to the old value, which means that in SSJ07, because of the poorer spectral window, we used an incorrect value corresponding to the one-day alias on the right side of the correct peak. This is probably the main reason of the different results. An incorrect value of f_4 can modify the multi-sinusoidal fits and thus slightly modify the phases of f_1 and f_2 as well.

² When we consider only f_1 and f_2 in the multi-sinusoidal fits instead of four frequencies, the results are almost identical to those reported in panels 3A to 4B of Fig. 9. When we use only Johnson-B-filter data, the main difference is that the period of the sinusoidal component of f_1 increases by 7%. When we do not use statistical weights, we obtain the largest difference, with the amplitude of the sinusoidal component of f_2 reduced from 9.4 to 5.4 s, while all other parameters remain about the same.

5. V391 Peg b: real planet or false detection ?

Whether V391 Peg b is a real planet or a false detection is an open question. The O–C diagrams of f_1 and f_2 provide arguments in favour and against the presence of V391 Peg b.

1) f_1 : considering the period up to 2009.0, the O–C diagram of f_1 still has a sinusoidal component that can be explained by the presence of a giant planet with a minimum mass of $3.5 M_{\text{Jup}}$, orbiting V391 Peg in 3.1 years at a distance of 1.7 AU. However, the behavior of f_1 after 2009.0 shows that this is more complex, and we see from Fig. 8 and 9 that a simple two-component fit of the O–C data is not enough to interpret the whole data set up to 2012. Using two sinusoids with different periods allows us to fit the O–C data up to 2010 or 2011, but the quality of the fit is much poorer. When we use two sinusoids, the period of the sine wave corresponding to the planet (Fig. 9/5B) is longer than the period obtained with a parabola plus a sine wave (Fig. 9/3B).

2) f_2 : up to 2009.0, the O–C diagram of f_2 also shows a sinusoidal component, but now, unlike SJJ07, the period and the amplitude differ from f_1 by $\sim 20\%$ and $\sim 36\%$, respectively. The new data support the previous identification of f_2 as an $l=1$ mode, and this implies that frequency splitting due to stellar rotation must be at work. Regardless of whether our detection of f_2^- is real, these modes split by stellar rotation must be there, close to f_2 , and this is a source of noise for the O–C computations of f_2 . This argument makes the O–C results from f_1 (which is an $l=0$ mode) more reliable, and this is one of the reasons why the presence of the planet cannot be excluded. At the same time, this argument can partially explain the discrepancies between the O–C diagrams of f_1 and f_2 .

3) f_1+f_2 : when we try to fit the whole set of O–C data using a sine wave plus a longer-period sinusoid for f_1 and a parabola for f_2 (panels 5 and 6 of Fig. 9), we see that the sine wave corresponding to the planet is very similar for f_1 and f_2 in terms of period, amplitude, and phase (panels 5B and 6B of Fig. 9). Although these fits are of poor quality, it is possible to obtain a substantial improvement when we use both pulsation frequencies together (Fig. 10). If we interpret this effect with the presence of the planet, we obtain a minimum mass of $1.8 M_{\text{Jup}}$, while the orbital period and distance, 3.1 years and 1.65 AU, do not change much with respect to the values obtained previously.

In conclusion, while in SJJ07 the presence of a planet orbiting V391 Peg was robustly and independently suggested by the two main pulsation modes of the star, these two modes now give contradictory indications. A sinusoidal component is still visible in the O–C diagrams of both f_1 and f_2 , but the parameters of the two sinusoids are different in general. The presence of a planet orbiting V391 Peg is clearly much less robust than before, although it cannot be entirely excluded.

The peculiar behavior of f_1 with a quite sudden change of sign of its time derivative after 2008 suggests that pulsation timing is a delicate method, with aspects that are still unclear and are likely related to nonlinear pulsation effects. As a consequence, the reliability of the O–C method to find low-mass companions should be questioned, without forgetting, however, that for sdB stars we have at least two cases in which the presence of a stellar companion was detected through pulsation timing (Barlow et al. 2011a; Otani et al. 2017), and in one case, for CS 1246, this detection was confirmed by radial velocity (RV) measurements (Barlow et al. 2011b). With respect to V391 Peg, the O–C detection was easier in both cases because of the much higher companion mass, and for CS 1246, also because of the much shorter orbital period of ~ 14 days, which meant no problems with the long-term variation of the pulsation period. Unlike

CS 1246, which exhibits a single large-amplitude radial mode, and EC 20117-4014, which shows three low-amplitude pulsation modes with frequency separations of ~ 250 and $\sim 680 \mu\text{Hz}$ (Otani et al. 2017), with V391 Peg we have the additional difficulty that all four pulsation modes are concentrated within $86 \mu\text{Hz}$, which makes it more difficult to measure the phases accurately.

In order to confirm or definitively reject the presence of V391 Peg b, an independent confirmation with another method is needed. Given that Gaia astrometry is not accurate enough at a distance of about 1400 pc, spectroscopic RVs seem the most natural way to proceed. However, the RV “noise” produced by the pulsations is a serious concern and can easily reach several hundred m/s, while the expected planetary signal is no more than 100 m/s. Given the very different time scales, it is in principle possible to remove or reduce the noise due to the pulsations, provided that we know the Fourier spectrum and the main pulsation modes in detail. This is true for the high-frequency part of the spectrum (the p -modes), which is relatively simple, with only two dominant modes that have similar periods. The noise due to the p -modes can be reduced by choosing an exposure time close to an integer multiple of ~ 350 s. For the g -modes, the situation is more complicated as the low-frequency part of the Fourier spectrum is not well known (see next section). The noise can be reduced by averaging the results obtained from different spectra taken in the same epoch at different pulsation phases. A great help for a precise determination of the g -modes may come from TESS (Transiting Exoplanet Survey Satellite, Ricker et al. 2016), which can observe V391 Peg continuously for 54 days in some years from now, with a sampling time of 20 or 120 s.

6. G-modes

G -modes were detected in V391 Peg by Lutz et al. (2009). Our new larger data set has been used to confirm this detection. Given that the g -modes are particularly disturbed by the atmospheric variations that act at similar frequencies, we selected a subset of high-quality data with a length of each single run of at least a few hours. This subset, which has a total duration of 192.8 hours spread over 5.8 years (between 2002 and 2008), was corrected for differential atmospheric extinction (the comparison stars are always much redder than the sdB) and analyzed. The amplitude spectrum in Fig. 11 shows two regions with an excess of power near 180 and $310 \mu\text{Hz}$ and three peaks that emerge from the noise at more than 5σ . The corresponding frequencies, amplitudes, and phases are listed in Table 3. The noise threshold, which was 4σ for the p -modes, was increased to 5σ because the spectrum is much more noisy in this region. After these three peaks were subtracted from the data, the lower panel of Fig. 11 shows that some residual power is still there, suggesting that further low-amplitude frequencies are likely present below the noise threshold. As anticipated in the previous section, in two years from now, TESS will be able to shed light on this part of the Fourier spectrum and likely measure the rotation period of the star, confirming or refuting the tentative rotation period of ~ 40 days suggested by the p -mode analysis in section 3.2.

7. Summary

Interpreting the new O–C results shown in Fig. 8 and 9 is more complicated than it was ten years ago. At that time, the very good agreement between the sine-wave component of f_1 and f_2 strongly supported the presence of a giant planet (SJJ07). Now, with many more data, this agreement is much more uncertain and

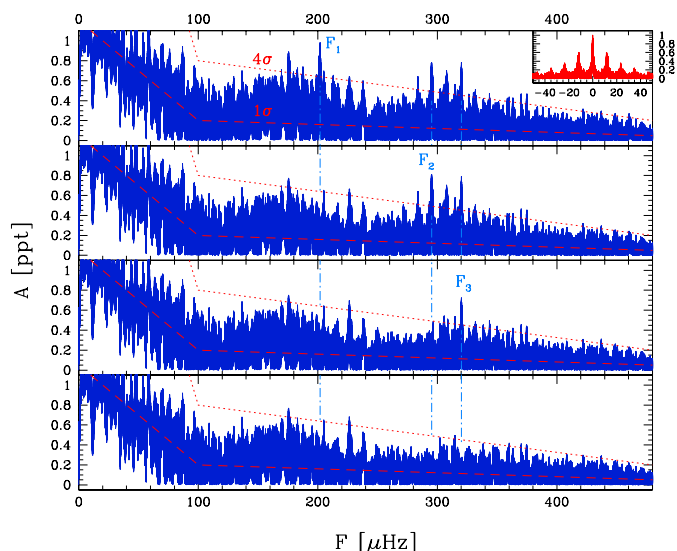


Fig. 11. *G*-mode amplitude spectrum using our best-quality runs between 2002 and 2008 (192.8 hours of observations in total). The upper right panel shows the spectral window (red), while the other panels from top to bottom show amplitude spectrum and residuals after one, two, and three whitening steps. We note an excess of power in two main regions near 180 and 310 μHz . After whitening, this excess of power is not completely removed near 180 μHz , suggesting that further low-amplitude frequencies are present in that region.

the presence of V391 Peg b is weaker and requires confirmation with an independent method. Like in SSJ07, a two-component fit (parabola + sine wave) still gives satisfactory results for both f_1 and f_2 , at least up to 2009. The sinusoidal components of f_1 and f_2 , however, now differ in period and amplitude by $\sim 20\%$ and $\sim 36\%$, respectively. Starting in phase, after two cycles the O-C sine wave of f_2 is antiphased with respect to f_1 . When we consider all the O-C data from 1999 to 2012, a two-component fit is in general not satisfactory. For f_1 , we tried to fit the O-C data with a double sine wave, corresponding to a sinusoidal behavior of \dot{p}_1 . The result is a very poor fit. However, this solution produces a certain agreement between the sinusoidal components of f_1 and f_2 .

The change in sign of the time derivative of the main pulsation period near 2009 is an intriguing phenomenon that is difficult to explain. Nonlinear interactions between pulsation modes seem the most natural explanation, but the $l=0$ identification (Silvotti et al. 2010), which is confirmed by the new data, does not help as we cannot invoke resonant mode coupling between the components of a multiplet nor resonance between modes linked by linear combinations that we do not see. The irregular behavior of f_1 agrees to a certain extent with recent *Kepler* results, which showed that sdB pulsation frequencies are in general less stable than previously believed. The *Kepler* results are mostly focused on *g*-modes, but a similar behavior seems also relatively common for the *p*-modes. At least this is suggested by our results.

The $l=1$ identification for f_2 (Silvotti et al. 2010) is also confirmed by the new data (or at least l must be >0). A retrograde mode is detected, although at the limit of our detection threshold, and this suggests a stellar rotation period of about 40 days.

Using only the data up to 2009.0, we can improve our previous measurements of \dot{p} for f_1 and f_2 and obtain $\dot{p}_1 = (1.34 \pm 0.04) \times 10^{-12}$ and $\dot{p}_2 = (1.62 \pm 0.22) \times 10^{-12}$. The order of magnitude of these numbers is in agreement with theoretical expectations for evolved models of extreme horizontal branch stars

(Charpinet et al. 2002), and their positive sign would normally be interpreted as an indicator of a stellar expansion. At least for f_1 , however, the change in curvature near 2009 implies that these numbers are not simply or directly related to the evolutionary timescales expected from theory, and the situation is more complicated.

Finally, the new data confirm that V391 Peg is a hybrid pulsator, showing both *p*- and *g*-modes. The next opportunity for a more detailed study of this star, and in particular for the study of the low-frequency part of its Fourier spectrum, is given by the TESS mission, which may observe V391 Peg continuously for 54 days in about two years from now. With a better knowledge of the Fourier spectrum at low frequencies as well, it should be easier to confirm or reject the presence of a planet orbiting V391 Peg by measuring the spectroscopic radial velocities of the star.

Acknowledgements. We thank Elia Leibowitz, who made the data collected at the Wise Observatory available to us, Christopher D. J. Savoury for helping us with the ULTRACAM observations and data reduction, and Wen-Shan Hsiao for contributing the Lulin data. We also thank Patrick Lenz for providing us with a modified version of period04, which facilitated the error estimation from the MC simulations. V. S. D. and ULTRACAM are supported by STFC grant ST/J001589/1. L. M. was supported by the the Hungarian National Research, Development and Innovation Office (NKFIH) grant PD-116175 and the János Bolyai Research Scholarship of the Hungarian Academy of Sciences.

References

- Almeida, L., Jablonski, F., & Rodrigues, C. 2013, *ApJ*, 766, 11
 Applegate, J. H. 1992, *ApJ*, 385, 621
 Baran, A. S., Zola, S., Blokesz, A., Østensen, R. H., & Silvotti, R. 2015, *A&A*, 577, A146
 Barlow, B. N., Dunlap, B. H., & Clemens, J. C. 2011a, *MNRAS*, 414, 3434
 Barlow, B. N., Dunlap, B. H., & Clemens, J. C. 2011b, *ApJ*, 737, L2
 Barnes, T. G. III, & Moffett T. J. 1975, *AJ*, 80, 48
 Bear, E., & Soker N. 2014, *MNRAS*, 444, 1698
 Beuermann, K., Hessman, F. V., Dreizler, S., et al. 2010, *A&A*, 521, L60
 Beuermann, K., Dreizler, S., Hessman, F. V., & Deller, J. 2012, *A&A*, 543, A138
 Bours, M. C. P., Marsh, T. R., Parsons, S. G., et al. 2016, *MNRAS*, in press
 Charpinet, S., Fontaine, G., Brassard, P., & Dorman B. 2002, *ApJSS* 140, 469
 Charpinet, S., Fontaine, G., Brassard, P., et al. 2011, *Nature*, 480, 496
 Compton, D. L., Bedding, T. R., Murphy, S. J., & Stello, D. 2016, *MNRAS*, 461, 1943
 Dalessio, J., Provencal, J. L., & Shipman, H. L. 2015, *ASPC*, 493, 157
 Eastman, J., Siverd, R., & Gaudi, S. 2010, *PASP*, 122, 935
 Geier, S., Schaffenroth, V., Drechsel, H., et al. 2011, *ApJ*, 731, L22
 Heber, U. 2016, *PASP*, 128, 966
 Hinse, T., Lee, J.-W., Goździewski, K., Horner, J., & Wittenmyer, R. A. 2014, *MNRAS*, 438, 307
 Kepler, S. O., Winget, D. E., Nather, R. E., et al. 1991, *ApJ*, 378, L45
 Konacki, M., & Wolszczan, A. 2003, *ApJ*, 591, L147
 Lanza, A. F. 2006, *MNRAS*, 369, 1773
 Ledoux, P. 1951, *ApJ*, 114, 373
 Lee, J.-W., Hinse, T. C., Youn, J.-H., & Han, W. 2014, *MNRAS*, 445, 2331
 Lenz, P., & Breger, M. 2005, *Comm in Asteroseismology*, 146, 53
 Lohr, M. E., Norton, A. J., Anderson, D. R., et al. 2014, *A&A*, 566, A128
 Loumos, G. L., & Deeming, T. J. 1977, *Ap&SS*, 56, 285
 Lutz, R., Schuh, S., & Silvotti, R. 2009, *A&A*, 496, 469
 Murphy, S. J., Bedding, T. R., Shibahashi, H., Kurtz, D. W., & Kjeldsen, H. 2014, *MNRAS* 441, 2515
 Murphy, S. J., Bedding, T. R., & Shibahashi, H. 2016a, *ApJ*, 827, L17
 Murphy, S. J., Shibahashi, H., & Bedding, T. R. 2016b, *MNRAS*, 461, 4215
 Østensen, R., Solheim, J.-E., Heber, U., et al. 2001, *A&A*, 368, 175
 Østensen, R. H., Reed, M. D., Baran, A. S., & Telting, J. H., 2014, *A&A*, 564, L14
 Otani, T., Oswalt, T. D., Lynas-Gray, A. E., et al. 2017, *ApJ* submitted, arXiv:1708.06029
 Qian, S.-B., Zhu, L.-Y., Zola, S., et al. 2009, *ApJ*, 695, L163
 Qian, S.-B., Zhu, L.-Y., Liu, L., et al. 2010, *A&SS*, 329, 113
 Qian, S.-B., Shi, G., Zola, S., et al. 2013, *MNRAS*, 436, 1408
 Randall, S. K., Fontaine, G., Brassard, P., & Bergeron, P. 2005, *ApJSS*, 161, 456
 Ricker, G. R., Vandarspek, R., Winn, J., et al. 2016, *Proc. SPIE*, 9904, 99042B
 Schaffenroth, V., Geier, S., Heber, U., et al. 2014, *A&A*, 564, A98
 Schaffenroth, V., Classen, L., Nagel, K. et al. 2014b, *A&A*, 570, A70

- Schaffenroth, V., Barlow, B. N., Drechsel, H., & Dunlap, B. H. 2015, *A&A*, 576, A123
- Schleicher, D. R. G., & Dreizler, S. 2014, *A&A* 563, A61
- Shibahashi, H., & Kurtz, D. W. 2012, *MNRAS*, 422, 738
- Shibahashi, H., Kurtz, D. W., & Murphy, S. J. 2015, *MNRAS*, 450, 3999
- Silvotti, R., Janulis, R., Schuh, S., et al. 2002, *A&A*, 389, 180
- Silvotti, R., Bonanno, A., Bernabei, S., et al. 2006, *A&A*, 459, 557
- Silvotti, R., Schuh, S., Janulis, R., et al. 2007, *Nature*, 449, 189 (SSJ07)
- Silvotti, R. 2008, *ASPC*, 392, 215
- Silvotti, R., Randall, S. K., Dhillon, V. S., et al. 2010, *AN*, 331, 1034
- Silvotti, R., Szabó, R., Degroote, P., Østensen, R. H., & Schuh, S. 2011, *AIPC*, 1331, 133
- Silvotti, R., Charpinet, S., Green, E., et al. 2014, *A&A*, 570, A130
- Sterken, C. 2005, *ASPC*, 335, 3
- Telting, J. H., Østensen, R. H., Baran, A. S., et al. 2012, *A&A*, 544, A1
- Völschow, M., Schleicher, D. R. G., Perdelwitz, V., & Banerjee, R. 2016, *A&A*, 587, A34
- Wolszczan, A., & Frail, D. A. 1992, *Nature*, 355, 145
- Zong, W., Charpinet, S., & Vauclair, G., 2016, *A&A*, 594, A46
- Zong, W., PhD Thesis 2017, Univ. of Toulouse,
<https://tel.archives-ouvertes.fr/tel-01434986/document>
- Zorotovic, M., & Schreiber, M. R. 2013, *A&A*, 549, A95